VEHICLE SIDESLIP ANGLE OBSERVERS

Joanny Stéphant*, Ali Charara*, Dominique Meizel*

* Laboratoire Heudiasyc UMR CNRS 6599
Université de Technologie de Compiègne
Centre de recherches de Royallieu BP 20259 - 60205 COMPIEGNE CEDEX, France
joanny.stephant@hds.utc.fr, ali.charara@hds.utc.fr, dominique.meizel@hds.utc.fr
Fax. 33 (0)3 44 23 44 77

Keywords: Sideslip angle, Observability, Nonlinear observation, Sliding mode observation, Vehicle model.

Abstract

This paper compares four observers of vehicle sideslip angle. The first is linear and uses a linear vehicle model. Next observers use an extended nonlinear model. The three nonlinear observers are: extended Luenberger observer, extended Kalman filter and sliding mode observer. Modelling and model simplification are described, and an observability analysis is performed for the entire vehicle trajectory. The paper also deals with three different sets of sensors. Comparison is first done by simulation, and then observers are used on experimental data.

1 Introduction

In vehicle development, knowledge of wheel-ground contact forces is important. The information is useful for security actuators, for validating vehicle simulators and for advanced vehicle control systems.
Braking systems and control systems must be able to stabilize the car during cornering. When subject to transversal forces, such as when cornering, or in the presence of a camber angle, tire torsional flexibility produces an aligning torque which modifies the original wheel direction. The difference is characterized by an angle known as "sideslip angle". This is a significant signal to determine the stability of the vehicle and it is the main transversal force variable.
Measuring sideslip angle would represent a disproportionate cost in the case of an ordinary car, and it must therefore be observed or estimated.
The literature describes several observers for sideslip angle. For example, Kiencke in [2] or [3] presents linear and nonlinear observers with a bicycle model. Venhovens [10], use a Kalman filter for a linear vehicle model.
The present study compares four observers for the sideslip angle on a conventional test with three different speeds. We are particularly concerned with the stability of the observers and the model as the vehicle approaches the linear dynamic limits. It also presents the results for three different sets of sensors: yaw rate; vehicle speed; yaw rate and vehicle speed together. We include some results concerning observability. Finally, it presents some experimental results obtained with the Heudiasyc experimental vehicle. All simulations have been performed using with Callas® software developed by SERA-CD (Vehicle engineering Research and Development Company), and all data processed with MATLAB® software.

2 Vehicle and simulator

2.1 STRADA

Figure 1: Heudiasyc laboratory experimental vehicle : STRADA

STRADA is the Heudiasyc Laboratory's test vehicle: a Citroën Xantia station-wagon equipped with a number of sensors. Tests use GPS, with longitudinal and lateral acceleration to trace the path and to determine whether the vehicle reaches linear approximation limits. The speed of center of gravity is calculated as the mean of the longitudinal speeds of the two rear wheels (odometry), and yaw rate obtained from the yaw rate gyrometer.

2.2 Callas®

Callas software is a realistic simulator validated by vehicle manufacturers including PSA, and research institutions including INRETS ("Institut national de recherche sur les transports et leur sécurité"). The Callas model takes into account vertical dynamics (suspension, tires), kinematics, elasto-kinematics, tire adhesion and aerodynamics.

3 Vehicle models

Lateral vehicle dynamics has been studied since the 50's. In 1956 Segel presented a vehicle model with three degrees of freedom in order to describe lateral movements including roll and yaw. If roll movement is neglected, a simple model known as the "bicycle model" is obtained. This model is currently used for studies of lateral vehicle dynamics (yaw and sideslip). A nonlinear representation of the bicycle model is shown in Figure 2. The different notations are indicated in the appendix

(section 9). Some simplifications are available for the different

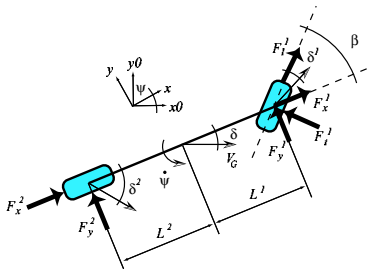

Figure 2: Bicycle model

models. Cornering stiffness is taken to be constant. But cornering stiffness increases with tire pressure. When the car turns, the mass transfer on the external wheels increases tire pressure. Figure 3 presents variations in cornering stiffness for different simulation speeds. The difference is less than 10%.
Tire/road forces are highly nonlinear. Various wheel-ground contact force models are to be found in the literature, including a comparison between three different models by Stéphant in [9]. In this paper, transversal forces are taken to be linear. This assumption is reasonable when lateral acceleration of the vehicle is less than $0.4g$ [4], limit of adhesion zone. Consequently, transversal forces can be written as:

$$F_y^i = C_{F\delta}^i . \delta^i \quad i = 1, 2 \tag{1}$$

Rear and front tire sideslip angles are calculated as:

$$\begin{cases} \delta^1 & = \beta - \delta - L^1 \frac{\dot{\psi}}{V_G} \\ \delta^2 & = -\delta + L^2 \frac{\dot{\psi}}{V_G} \end{cases} \tag{2}$$

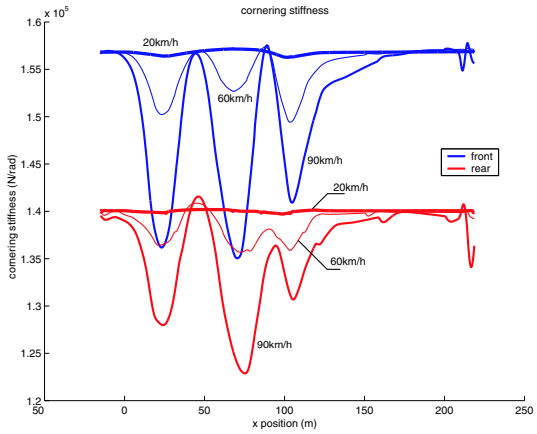

Figure 3: Right rear and front cornering stiffness for slalom at $20km.h^{-1}$, $60km.h^{-1}$ and $90km.h^{-1}$

3.1 Linear model - LM

Given the assumption of cornering at constant speed, with small steering angle and sideslip angle, the linear model is:

$$\begin{cases} \dot{\mathbf{X}} & = \mathbf{AX} + \mathbf{Bu} \\ \mathbf{Z} & = \mathbf{CX} \end{cases} \tag{3}$$

with $\mathbf{X} = (\delta \quad \dot{\psi})^T, \mathbf{u} = \beta, \mathbf{B} = \begin{pmatrix} \frac{C_{F\delta}^1}{m_v V_G} & \frac{C_{F\delta}^1 L^1}{I_{zz}} \end{pmatrix}^T$

$$\mathbf{A} = \begin{pmatrix} \frac{-C_{F\delta}^1 - C_{F\delta}^2}{m_v V_G} & \frac{-C_{F\delta}^1 L^1 + C_{F\delta}^2 L^2}{m_v (V_G)^2} - 1 \\ \frac{-C_{F\delta}^1 L^1 + C_{F\delta}^2 L^2}{I_{zz}} & \frac{-C_{F\delta}^1 (L^1)^2 - C_{F\delta}^2 (L^2)^2}{I_{zz} V_G} \end{pmatrix}$$

3.2 Nonlinear model - NLM

The nonlinear bicycle model is described as:

$$\begin{cases} \dot{\mathbf{X_1}} = & \frac{1}{m_v}[\mathbf{U_2} cos(\mathbf{X_2} - \mathbf{U_1}) + \mathbf{U_3} cos(\mathbf{X_2}) \\ & -C_{F\delta}^1(\mathbf{U_1} - \mathbf{X_2} - L^1 \frac{\mathbf{X_3}}{\mathbf{X_1}}) sin(\mathbf{X_2} - \mathbf{U_1}) \\ & +C_{F\delta}^2(-\mathbf{X_2} + L^2 \frac{\mathbf{X_3}}{\mathbf{X_1}}) sin(\mathbf{X_2})] \\ \dot{\mathbf{X_2}} = & \frac{1}{m_v \mathbf{X_1}}[-\mathbf{U_2} sin(\mathbf{X_2} - \mathbf{U_1}) - \mathbf{U_3} sin(\mathbf{X_2}) \\ & +C_{F\delta}^1(\mathbf{U_1} - \mathbf{X_2} - L^1 \frac{\mathbf{X_3}}{\mathbf{X_1}}) cos(\mathbf{X_2} - \mathbf{U_1}) \\ & +C_{F\delta}^2(-\mathbf{X_2} + L^2 \frac{\mathbf{X_3}}{\mathbf{X_1}}) cos(\mathbf{X_2})] - \mathbf{X_3} \\ \dot{\mathbf{X_3}} = & \frac{1}{I_{zz}}[L^1 \mathbf{U_2} sin(\mathbf{U_1}) - L^2 C_{F\delta}^2(-\mathbf{X_2} + L^2 \frac{\mathbf{X_3}}{\mathbf{X_1}}) \\ & +L^1 C_{F\delta}^1(\mathbf{U_1} - \mathbf{X_2} - L^1 \frac{\mathbf{X_3}}{\mathbf{X_1}}) cos(\mathbf{U_1})] \end{cases} \tag{4}$$

where the state vector is: $\mathbf{X} = (V_G \quad \delta \quad \dot{\psi})^T$ and the input vector: $\mathbf{U} = (\beta \quad F_l^1 \quad F_l^2)^T$

3.3 Extended nonlinear model - ENLM

In the extended nonlinear model, longitudinal forces and their first derivatives become state variables with a random walk dynamic (like constants parameters). This could be used for estimating longitudinal forces, as in [8].
The state vector becomes:
$\mathbf{X} = \left(V_G \quad \delta \quad \dot{\psi} \quad F_l^1 \quad \dot{F_l^1} \quad F_l^2 \quad \dot{F_l^2}\right)^T$ and the input vector: $\mathbf{U} = (\beta)$

$$\begin{cases} \dot{\mathbf{X_1}} = & \frac{1}{m_v}[\mathbf{X_4} cos(\mathbf{X_2} - \mathbf{U_1}) + \mathbf{X_6} cos(\mathbf{X_2}) \\ & -C_{F\delta}^1(\mathbf{U_1} - \mathbf{X_2} - L^1 \frac{\mathbf{X_3}}{\mathbf{X_1}}) sin(\mathbf{X_2} - \mathbf{U_1}) \\ & +C_{F\delta}^2(-\mathbf{X_2} + L^2 \frac{\mathbf{X_3}}{\mathbf{X_1}}) sin(\mathbf{X_2})] \\ \dot{\mathbf{X_2}} = & \frac{1}{m_v \mathbf{X_1}}[-\mathbf{X_4} sin(\mathbf{X_2} - \mathbf{U_1}) - \mathbf{X_6} sin(\mathbf{X_2}) \\ & +C_{F\delta}^1(\mathbf{U_1} - \mathbf{X_2} - L^1 \frac{\mathbf{X_3}}{\mathbf{X_1}}) cos(\mathbf{X_2} - \mathbf{U_1}) \\ & +C_{F\delta}^2(-\mathbf{X_2} + L^2 \frac{\mathbf{X_3}}{\mathbf{X_1}}) cos(\mathbf{X_2})] - \mathbf{X_3} \\ \dot{\mathbf{X_3}} = & \frac{1}{I_{zz}}[L^1 \mathbf{U_2} sin(\mathbf{U_1}) - L^2 C_{F\delta}^2(-\mathbf{X_2} + L^2 \frac{\mathbf{X_3}}{\mathbf{X_1}}) \\ & +L^1 C_{F\delta}^1(\mathbf{U_1} - \mathbf{X_2} - L^1 \frac{\mathbf{X_3}}{\mathbf{X_1}}) cos(\mathbf{U_1})] \\ \dot{\mathbf{X_4}} = & \mathbf{X_5} \\ \dot{\mathbf{X_5}} = & 0 \\ \dot{\mathbf{X_6}} = & \mathbf{X_7} \\ \dot{\mathbf{X_7}} = & 0 \end{cases} \tag{5}$$

3.4 Remarks

All models have been implemented in a discrete form with MATLAB software. The sampling rate is 20 ms.
The nonlinear and extended nonlinear systems are undefined when $V_G = 0\ m.s^{-1}$. In practice, there is a problem of divergence when $V_g < 1\ m.s^{-1}$. When speed is less than $1\ m.s^{-1}$, sideslip angle effects are negligible in comparison to the yaw rate.

4 Observers

Four different observers are used in this paper.

4.1 Linear observer (LO)

The linear observer used in this paper is a Luenberger observer [3]. It is applied to system described by equation (3).

4.2 Nonlinear observer (NLO)

$$\begin{cases} \dot{\mathbf{X}} &= \mathbf{f}(\mathbf{X},\mathbf{U}) \\ \mathbf{Z} &= \mathbf{C}(\mathbf{X}) \\ \dot{\widehat{\mathbf{X}}} &= \mathbf{f}(\widehat{\mathbf{X}},\mathbf{U}) + \mathbf{L}(\widehat{\mathbf{X}},\mathbf{U})(\mathbf{Z}-\widehat{\mathbf{Z}}) \\ \widehat{\mathbf{Z}} &= \mathbf{C}(\widehat{\mathbf{X}}) \end{cases} \tag{6}$$

$\mathbf{f}(\mathbf{X},\mathbf{U})$ and $\mathbf{C}(\mathbf{X})$ are nonlinear functions in state and input. After linearization, with a pole placement technique, it is possible to impose error dynamics. The system matrix of the closed-loop system has constant poles $\mathbf{G}$. The observer is stable.
The gain matrix of the observer is computed by:

$$\mathbf{L}(\widehat{\mathbf{X}},\mathbf{U}) = [\frac{\partial \mathbf{f}}{\partial \mathbf{X}}(\widehat{\mathbf{X}},\mathbf{U}) - \mathbf{G}][\frac{\partial \mathbf{C}}{\partial \mathbf{X}}(\widehat{\mathbf{X}})]^{\dagger} \tag{7}$$

with † is the pseudo-inverse: $[A]^{\dagger} = A^T(A.A^T)^{-1}$

4.3 Extended Kalman filter (EKF)

The Kalman filter has been applied and described in many studies. For example, Mohinder and Andrews [5] present a wide overview of Kalman filtering. In this paper, an extended Kalman filter with measured input is used. The error measurement covariance matrix R is determined by sensor variance. R is a diagonal matrix, measurements are independent. The error model covariance matrix Q is determined by model quality.

4.4 Sliding mode observer (SMO)

From [6], this kind of observer is useful when working with reduced observation error dynamics, for a finite time convergence for all observable states, and for robustness under parameter variations (with respect to conditions).

$$\begin{cases} \dot{\mathbf{X}} &= \mathbf{f}(\mathbf{X},\mathbf{U}) \\ \mathbf{Z} &= \mathbf{C}(\mathbf{X}) \\ \dot{\widehat{\mathbf{X}}} &= \mathbf{f}(\widehat{\mathbf{X}},\mathbf{U}) + \mathbf{\Lambda} sign_{eq}(\mathbf{Z}-\widehat{\mathbf{Z}}) \\ \widehat{\mathbf{Z}} &= \mathbf{C}(\widehat{\mathbf{X}}) \end{cases} \tag{8}$$

To cover chattering effects [1], the function $sign_{eq}$ is as follows:

$$sign_{eq}(x) = atan(x) * 2/\pi \tag{9}$$

5 Observability

5.1 Linear system

System describes by equation (3) is observable if the matrix $\mathcal{O} = (\mathbf{C} \quad \mathbf{CA} \quad \mathbf{CA^2} \quad \dots \quad \mathbf{CA}^{n-1})^T$ has a rank equal to n. The observability condition is given by:

$$C^1_{F\delta} L^1 \neq C^2_{F\delta} L^2 \tag{10}$$

This condition is equivalent to "neutral steer" property of the vehicle. In the simulation case the system is observable because (10) $\Leftrightarrow 183591 \neq 235637$

5.2 Nonlinear system

In the nonlinear case, the observability definition is local and uses the Lie derivative [7]. For system described by equation (4) and sensor set Z_3 defined in section (**??**) the observability function is:

$$\mathbf{o} = \begin{pmatrix} h_1(\mathbf{X}) \\ (L_f h_1)(\mathbf{X},\mathbf{U}) \\ (L_f^2 h_1)(\mathbf{X},\mathbf{U}) \\ h_2(\mathbf{X}) \\ (L_f h_2)(\mathbf{X},\mathbf{U}) \\ (L_f^2 h_2)(\mathbf{X},\mathbf{U}) \end{pmatrix} \tag{11}$$

where : $h_1(\mathbf{X}) = X_1 = V_G$ and $h_2(\mathbf{X}) = X_3 = \dot{\psi}$
If this function is invertible at the current state and input, the system is observable. This function is invertible if the jacobian matrix $\mathbf{O}$ has a full rank.

$$\mathbf{O} = \frac{d}{d\mathbf{X}}\mathbf{o} \tag{12}$$

For system dsecribes by equation (5) the observability study is the same.
For the nonlinear and extended nonlinear systems, the rank of the observability matrix is respectively

$$3 = n_{NLM} \quad or \quad 7 = n_{ENLM}$$

along the path. The computation is performed at each time step with the different sensor sets.

6 Simulation Results

6.1 Remarks

Values in the different tables and figures are calculated along the full path from the **maximum error** and the **mean error** between the estimated state and the measured one. Those errors are normalized by the maximum of state value along the full path. For example, figure 4 give the error max and mean for the sideslip angle models and observers. Table 1 give the maximum value of sideslip angle calculated by Callas. On figure 7b) normalized maximum error of SMO for sideslip angle is: 30 %. The normalized mean error is therefore 9 %.

6.2 Simulation conditions

Simulations were performed using three sets of sensors:
• Z_1: Yaw rate only
• Z_2: Speed of center of gravity only
• Z_3: Speed of center of gravity and yaw rate together
Tests took place in a chicane at three different speeds: $20km.h^{-1}$, $60km.h^{-1}$ and $90km.h^{-1}$.

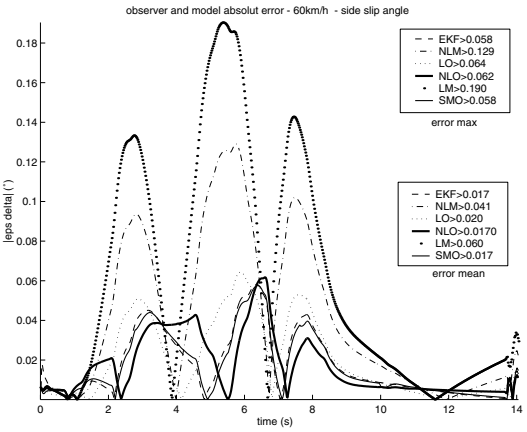

Figure 4: Sideslip angle error, $60km.h^{-1}$, Z_3

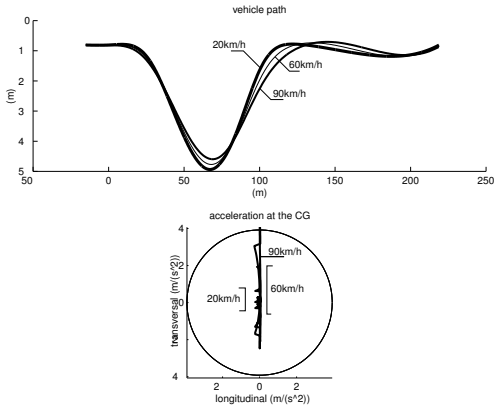

Figure 5: Path and acceleration for chicane at $20km.h^{-1}$, $60km.h^{-1}$, $90km.h^{-1}$

Figure 5 presents the simulation path and acceleration for the different speeds. Table 1 gives the maximum values for speed of center of gravity, yaw rate and sideslip angle at the different speeds. Figure 6 shows the sideslip angle calculated using the linear and nonlinear ($F_x^i \equiv 0$) models and observers results. In Figure 5 it can be seen that longitudinal acceleration is close to zero, meaning that longitudinal forces are virtually nonexistent. The simulation by the nonlinear model with zero force input seems to be a good simulation. Table 2 shows that a good

	$max(\dot{\psi})$ $^o.s^{-1}$	$max(V_G)$ $m.s^{-1}$	$max(\delta)$ ^{o}
$20km.h^{-1}$	2.8	5.6	0.7
$60km.h^{-1}$	7.3	16.6	0.19
$90km.h^{-1}$	9.9	24.9	0.21

Table 1: Maximum values for chicanes simulations

approximation of speed is obtained from the nonlinear model. The error is less than 1 % for the three speeds (mean and max). Throughout the path the Callas simulator driver aims to maintain a constant speed. There are only small speed variations.
The greater the speed, the greater the yaw rate estimation error. From table 2, mean error is 5 % at 60 $km.h^{-1}$. At 90 $km.h^{-1}$, it is 10 %. This indicates that the models are valid in respect of lateral movements. As regards sideslip angle, neither model is accurate. It would appear that observers are necessary to correct the estimations.

(%)	$\frac{max(\lvert\epsilon_{\dot{\psi}}\rvert)}{max(\dot{\psi})}$			$\frac{max(\lvert\epsilon_{V_G}\rvert)}{max(V_G)}$			$\frac{max(\lvert\epsilon_{\delta}\rvert)}{max(\delta)}$		
$km.h^{-1}$	20	60	90	20	60	90	20	60	90
LM	1.5	17	39	-	-	-	10	99	257
NLM	2.5	18	40	0.5	0.6	0.7	1.1	67.2	236
(%)	$\frac{mean(\lvert\epsilon_{\dot{\psi}}\rvert)}{max(\dot{\psi})}$			$\frac{mean(\lvert\epsilon_{V_G}\rvert)}{max(V_G)}$			$\frac{mean(\lvert\epsilon_{\delta}\rvert)}{max(\delta)}$		
$km.h^{-1}$	20	60	90	20	60	90	20	60	90
LM	0.6	4.8	10	-	-	-	3.1	31	78
NLM	0.8	5.1	10	0.3	0.3	0.4	0.6	21	71

Table 2: Models error for full simulation - max/mean

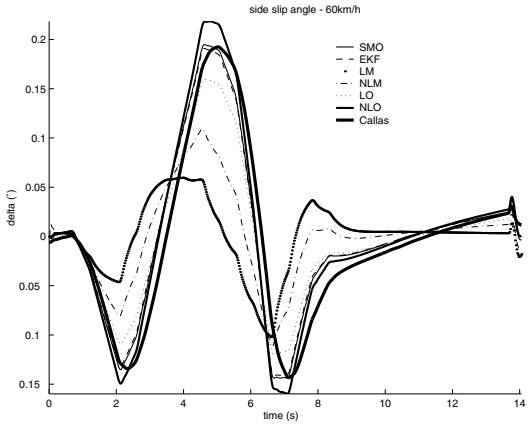

Figure 6: Sideslip angle, $60km.h^{-1}$, Z_3

6.3 Observers results for chicane at 20, 60 and 90$km.h^{-1}$

•**Observers results for chicane at 20** $km.h^{-1}$
Figure 7a) shows the results of the sideslip angle observation at $20km.h^{-1}$. At 20 $km.h^{-1}$, all nonlinear observers are highly accurate in respect of sideslip angle (less than 1 % in max and mean).

•**Observers results for chicane at 60** $km.h^{-1}$
Figure 6 shows simulated and estimated sideslip angle at 60 $km.h^{-1}$. A comparison of table 2 and figure 7b) shows that observers give a better approximation of sideslip angle than models. If the measurement is only the speed of the center of gravity, observers improve the accuracy of the sideslip angle. But yaw rate measurement, with its substantially better mean accuracy (10 %), would appear indispensable.

•**Observers results for chicane at 90** $km.h^{-1}$
Figure 7c) show the results of the sideslip angle observation at $90km.h^{-1}$. The same remarks can be made as for 60 $km.h^{-1}$. Two explanations can be given for the errors. Table 2 shows that the accuracy of the model decreases as speed increases. The second explanation is that at 90 $km.h^{-1}$ demands on tires are large. The maximum error occurs at maximum transversal acceleration, when we reach the limit of linear approximation.

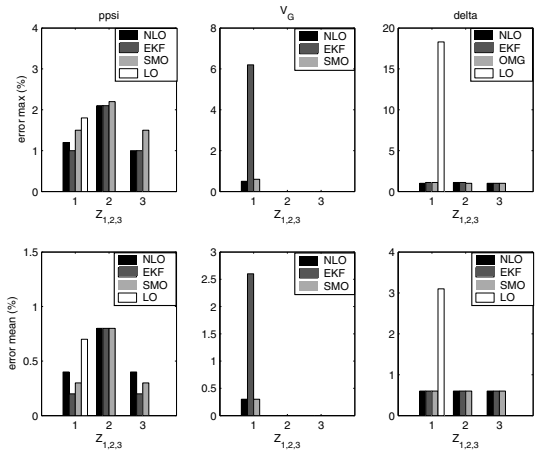

a) Observers error for chicane at $20km.h^{-1}$ - max/mean

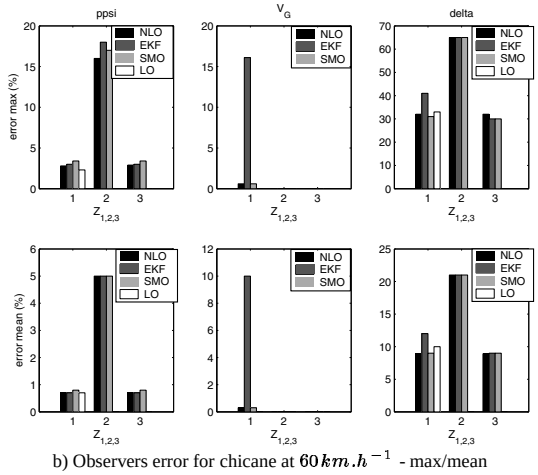

b) Observers error for chicane at $60km.h^{-1}$ - max/mean

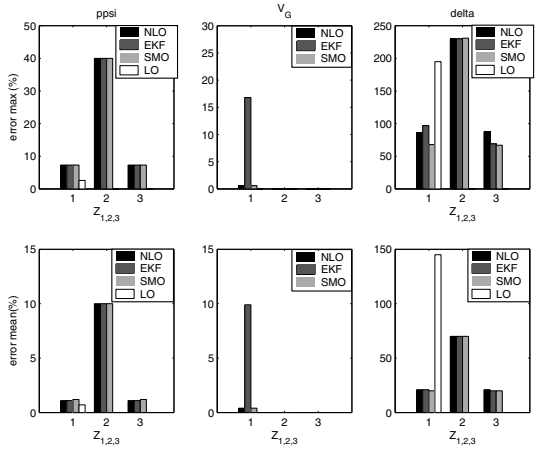

c) Observers error for chicane at $90km.h^{-1}$ - max/mean

Figure 7: Observer error for chicane Chicane at 20, 60 and $90km.h^{-1}$ - max/mean

7 Road tests

7.1 Test conditions

Figure 8 presents the vehicle trajectory and acceleration during the tests. Table 3a) gives the maximum values for vehicle speed, taken as the mean of longitudinal speeds of the two rear wheels, and maximum yaw rate.

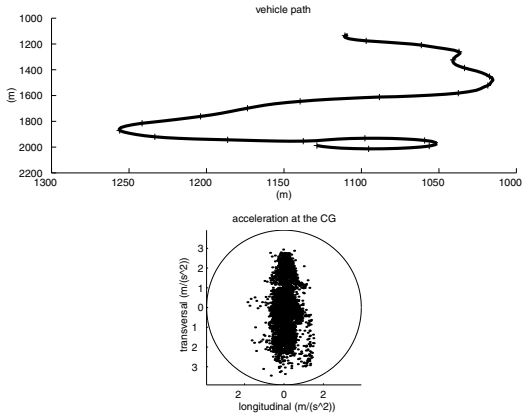

Figure 8: Path and acceleration

7.2 Results

Table 3 gives maximum and mean error, normalized by maximum value, for linear and extended nonlinear systems along the test path.

$max(\dot{\psi})$ $^{o}.s^{-1}$	$max(V_G)$ $m.s^{-1}$
16.6	14.0

a) Maximum measurement values for experimental test

(%)	$\frac{max(\lvert\epsilon_{\dot{\psi}}\rvert)}{max(\dot{\psi})}$	$\frac{max(\lvert\epsilon_{V_G}\rvert)}{max(V_G)}$
LM	23	-
NLM	34	28
(%)	$\frac{mean(\lvert\epsilon_{\dot{\psi}}\rvert)}{max(\dot{\psi})}$	$\frac{mean(\lvert\epsilon_{V_G}\rvert)}{max(V_G)}$
LM	8.2	-
NLM	5.4	11.2

b) Model error - max/mean

Table 3: a) Maximum measurement values for experimental test b) Model error - max/mean

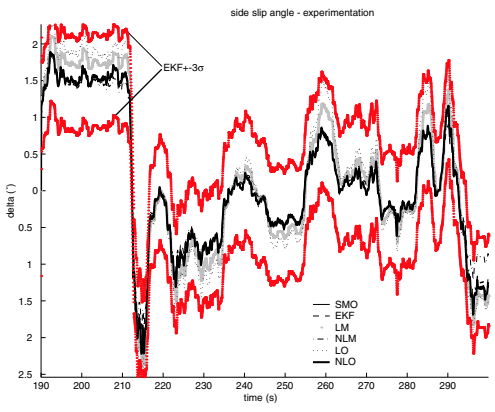

Figure 9: Sideslip angle, Z_3

Figure 8 shows that longitudinal acceleration is not negligible, and that longitudinal forces are present. The NLM simulation

has zero force input. This explains the error obtained in the nonlinear model. The approximation of yaw rate obtained from the models has a mean error lower than 10 %.
Because STRADA does not have a sideslip angle sensor, we do not have a validation measure for sideslip angle. Figure 10 gives the maximum and mean error for yaw rate and velocity estimations. Figure 9 presents the sideslip angle observed during the tests, and the confidence interval at 3σ for the EKF.

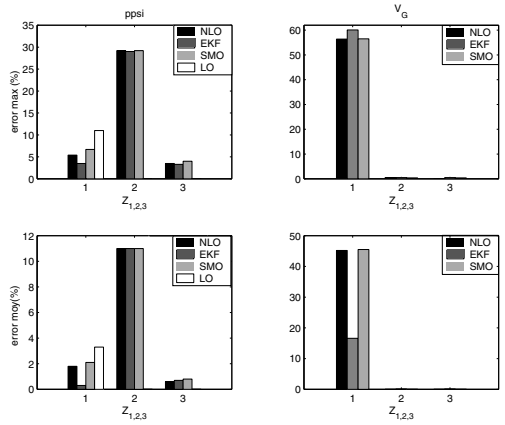

Figure 10: Observers error - max/mean

Figure 9 shows that the linear observer is the least accurate because constant speed hypothesis is false along the experimental path. All observers are in the 3σ bandwidth of EKF. The real sideslip angle is in this confidence interval. The three nonlinear observers are close to each other.

8 Conclusion

This study deals with four different sideslip angle observers with three sets of sensor. It consists of two parts. The first part includes simulation results. We can see from the results that the measurement of the speed of center of gravity is not a determinant variable in the estimation of sideslip angle. But this measure gives a little estimation improvement. The EKF applied with the sensor set Z_1 gives less accurate estimations than NLO and SMO. There are some convergence problems with the NLO with non-optimal initial states. Nonlinear sideslip angle observers (NLO, EKF and SMO) give approximately the same results. All observers are satisfactory when lateral acceleration is low. In normal driving conditions, lateral acceleration is often low. Observers can provide a good estimation. Along the different paths, all observers are stable. They all represent transients qualitatively. Future studies will take into account the four wheels and vertical dynamics, as well as providing a better model for longitudinal forces.

Acknowledgments

This study was done in collaboration with the research group "DIagnostic et Véhicules Avancés" financed by the Picardie region, and with the help of SERA-CD (http://www.sera-cd.com), within the framework of the "Action de Recherche pour une COnduite sécurisée" project, financed by the PREDIT program.

9 Appendix - Notations

$C_{F\delta}^{1,2}$	Front, rear wheel cornering stiffness $N.rad^{-1}$
$F_x^{1,2}$	Longitudinal front, rear force in the vehicle frame N
$F_y^{1,2}$	Transversal front, rear force in the vehicle frame N
F_l^1	Longitudinal front force in the front wheel frame N
F_t^1	Transversal front force in the front wheel frame N
$L^{1,2}$	CG to front, rear axle distance m
V_G	Speed of center of gravity $m.s^{-1}$
X	State vector $\in \mathbb{R}^n$
Z	Measurement vector $\in \mathbb{R}^p$
β	Steering angle rad
δ	Vehicle sideslip angle rad
$\delta^{1,2}$	Front, rear wheel sideslip angle rad
$\dot{\psi}$	Yaw rate $rad.s^{-1}$

References

[1] S Chabraoui. "observateurs à modes glisssants dédiés aux systèmes possédant des singularités d'observation". *Journées Doctorales d'Automatique, Toulouse, France*, September 2001.

[2] U. Kiencke and A. Daiß. "observation of lateral vehicle dynamics". *Control Eng. Practice*, 5(8):1145–1150, 1997.

[3] Uwe Kiencke and Lars Nielsen. *"Automotive control system"*. Springer-Verlag, 2000.

[4] Daniel Lechner. *"Analyse du comportement dynamique des véhicules routiers légers : développement d'une méthodologie appliquée à la sécurité primaire"*. PhD thesis, École centrale de Lyon, Octobre 2001.

[5] S. Grewal Mohinder and P. Andrews Angus. *Kalman filtering theory and practice*. Prentice hall, 1993.

[6] Wilfrid Perruquetti and Jean-Pierre Barbot. *Sliding mode control in engineering*. Marcel Dekker, Inc., 2002.

[7] H Nijmeijer and A. J. Van der Schaft. *Nonlinear Dynamical Control Systems*. Springer-Verlag, 1990.

[8] Laura R. Ray. "nonlinear tire force estimation and road friction identification : Simulation and experiments". *Automatica*, 33(10):1819–1833, 1997.

[9] Joanny Stéphant, Ali Charara and Dominique Meizel. "force model comparison on the wheel-ground contact for vehicle dynamics". *Proc. IEEE Intelligent Vehicle Symposium - Versailles*, juin 2002.

[10] P.J.TH Venhovens and Karl Naab. "vehicle dynamics estimation using kalman filters". *Vehicle System Dynamics*, 32:171–184, 1999.